PERGAMON

International Journal of Multiphase Flow 25 (1999) 1033–1052

International Journal of Multiphase Flow

www.elsevier.com/locate/ijmulflow

Heat transfer enhancement by air injection in upward heated mixed-convection flow of water

G.P. Celata*, A. Chiaradia, M. Cumo, F. D'Annibale

ENEA, Energy Department, Via Anguillarese 301, I-00060 S.M. Galeria, Rome, Italy

Received 9 December 1998; received in revised form 26 May 1999

The Authors wish to add their wishes to the celebration of this important milestone, the 65th birthday of Professor Gad Hetsroni. Gad being among the founders of multiphase flow as a discipline, we actually cannot realize what this discipline could have been without the contribution of our friend. We wish Gad continued professional success, good health, and happiness in the years to come.

Abstract

The present paper reports on the possibility of enhancing the heat transfer rate in diabatic pipe water upflow using injection of air at the inlet of the heated channel. In turbulent upward mixed convection, the laminarization effect in the near-wall region is the main responsible of heat transfer reduction. Under these conditions, air injection was proved to enhance the heat transfer coefficient up to a factor of 10 in mixed-convection flow, simply as a consequence of turbulence increase and related suppression of the laminarization effect by air bubbles injected in the water flow. A specific series of experiments has been carried out with the aim of determining the flow pattern in the pipe using a Plexiglas tube. High speed movies of the flow allowed to evaluate the slip ratio, and then the void fraction, together with the identification of the flow pattern, which was mostly slug flow. The observed flow pattern showed how, in all cases, the gas phase caused a disturbance in the velocity profile in the near-wall region. The turbulence increase locally produced by air bubbles suppresses the laminarization effect, thus greatly enhancing the heat transfer coefficient.

Keywords: Heat transfer enhancement; Air injection; Upward mixed convection; Water flow

* Corresponding author. Fax: +39-06-3048-3026.
E-mail address: celata@casaccia.enea.it (G.P. Celata)

0301-9322/99/$ - see front matter
PII: S0301-9322(99)00059-2

1. Introduction

Heat transfer from a heated wall to a liquid may be poor for laminar or low-Reynolds single-phase flow, or for upward mixed-convection heated flow. For all the cases where operating conditions do not allow high flow velocity, and/or higher heat transfer rates are required, heat transfer enhancement techniques are commonly used. Typically, passive techniques as swirl flows are used to increase the turbulence of the flow, and, consequently, the heat transfer coefficient. For laminar flow of liquid in pipes, twisted tapes, wire coils and wire matrix inserts have been used in the past (Du Plessis and Kroger, 1987; Uttarwar and Raya Rao, 1985; Oliver and Aldington, 1986). These systems, even if they do promote turbulence for low liquid velocity, present some drawbacks: pressure drop increase, presence of obstacles to the flow in case of a break of the inserts, larger fouling in case of not clean fluids.

In the present work, an alternative method is presented, based on the injection of gas into the liquid, with the aim of promoting turbulence, mainly at low flow velocity and in mixed-convection flow. The experimental study is performed using a vertical tube, uniformly heated by Joule effect (DC heating), internally cooled with water. The heat transfer coefficient is obtained for water flow with and without gas injection, for a wide range of conditions.

The results obtained show that the introduction of a small gas flow rate may lead to a remarkable increase in the heat transfer coefficient. The effect is more evident for upward mixed-convection heated flow, and it tends to decrease as the thermodynamic conditions of the liquid approach those characteristic of the onset of nucleate boiling.

2. The experimental facility

The experimental facility, sketched in Fig. 1, is made up of two loops: a demineralized water loop and a gas loop (air). From a separator-tank the water flow goes through a piston pump (maximum flow rate 1800 kg/h, residual pulsation below 2.5%), is filtered, pre-heated and delivered to the bottom end of the vertical test channel, through which is directed to the tank. Pressurized air is injected into the water flow before entering the test section. The Air flow rate is regulated through a sonic disc, at which critical flow conditions occur, so that the flow rate depends only on the upstream thermodynamic conditions. Two different sonic discs are used, whose diameters are 0.12 and 0.19 mm, respectively. Three different modes of gas injection are used, as sketched in Fig. 2: (a) very far from the test section inlet (air — 'F' tests), (b) central injection of air, normal to the water flow (air — 'X' tests), and (c) annular-like air injection (air — 'Y' tests); (b) and (c) types of air injection are located close to the test section inlet (20 cm, equivalent to 7.7 diameters).

The test section is a vertical 316-type stainless steel tube, thermally insulated and electrically heated by Joule effect (DC heating). The water flow is upward. The test section characteristics are:

inner diameter, D	26 mm
thickness, s	1 mm
total length, L_{tot}	1 m
heated length, L	0.5 m
max thermal power, W_{max}	7.5 kW (1400 A)

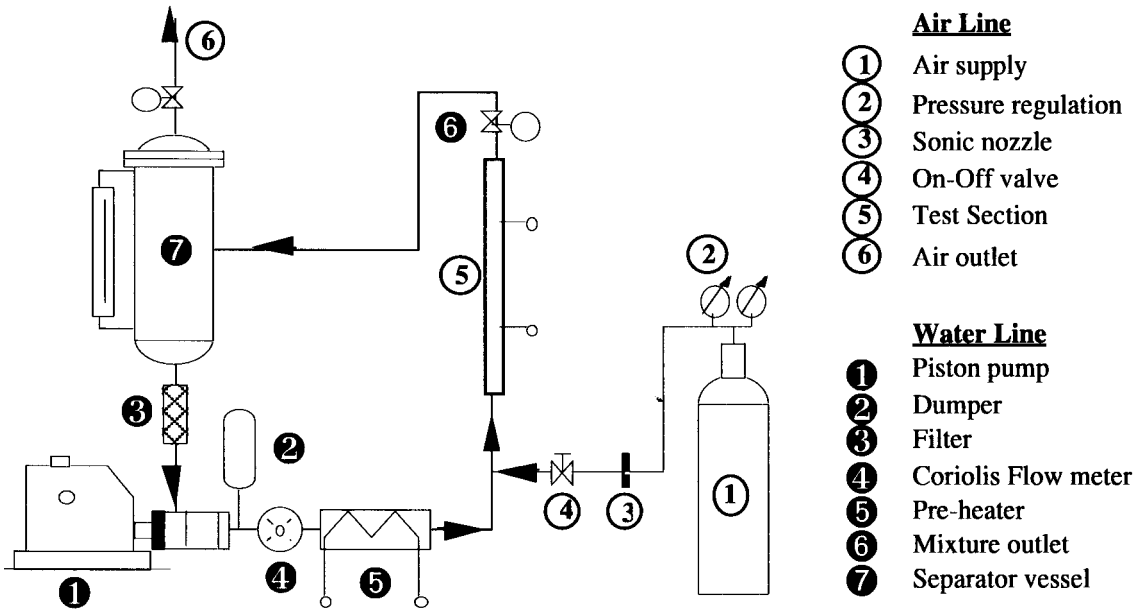

Fig. 1. Schematic of the experimental facility.

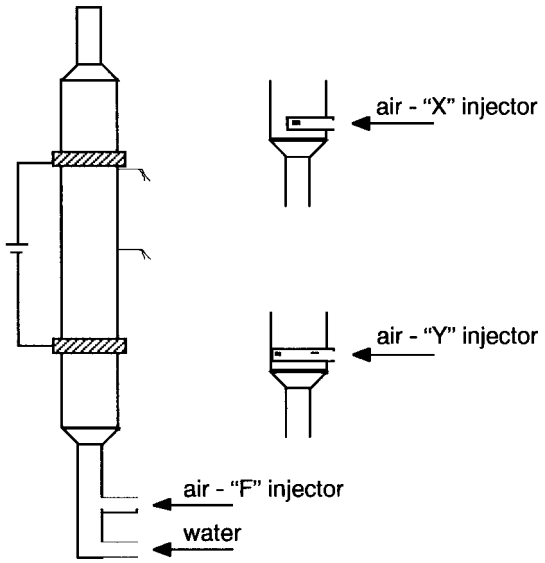

Fig. 2. Schematic of the test section.

Wall temperatures are measured using two K-type 0.5 mm thermocouples. Their hot junction is placed 0.5 mm inside the tube wall thickness. The inner wall temperature is calculated correcting the thermocouple readings by means of the Fourier equation. The wall thermocouples are located at 25 and 40 cm from the bottom copper clamp. The water temperature is measured at the test section inlet, outlet and middle sections (same kind of thermocouples). The inlet and outlet pressures are measured using sealed pressure transducers, while the mass flow rate is measured using a Coriolis-meter (12–250 kg/h), Danfoss Mass 100 DI3 type, and a turbine flow meter (200–2000 kg/h), Faure-Herman 25-2 type. The air flow rate is obtained by measuring pressure (using a Druck Ptx 100/IS transducer) and temperature (using K-type thermocouple) upstream the sonic disc, and using the following equation:

$$G_c = \left[\gamma p_0 \rho_0 \left(\frac{2}{\gamma + 1} \right)^{\frac{\gamma+1}{\gamma-1}} \right]^{1/2} \tag{1}$$

where G_c is the critical mass flux, γ the c_p/c_v ratio (with c_p and c_v the specific heats at constant pressure and volume), p_0 the stagnation pressure and ρ_0 the stagnation density. Eq. (1) provides the gas critical mass flux through an orifice, for a downstream pressure lower than the critical pressure, p_c, given by the formula:

$$p_c = p_0 \left(\frac{2}{\gamma + 1} \right)^{\gamma/\gamma-1} \tag{2}$$

Accounting for the possible error in pressure, temperature and sonic disc diameter measurements, the uncertainty in the air flow rate obtained from Eq. (1) is less than 2.3%.

The test conditions are the following:

inlet pressure, p_{in}	from 0.1 to 0.52 MPa
inlet liquid phase temperature, $T_{l,in}$	from 15 to 108°C
liquid mass flow rate, Γ_l	from 80 to 850 kg/h
liquid mass flux, G_l	from 40 to 490 kg/m^2 s
gas mass flow rate, Γ_g	from 40 to 1800 g/h
Reynolds number, $Re = GD/\mu$	from 1160 to 24000
heat flux, q''	from 4.8 to 178 kW/m^2
quality, x	from 0 to 0.01.

To get direct information about the flow pattern in the pipe for the two-phase flow after air injection and its possible effect on heat transfer, a specific series of experiments is carried out without heating, replacing the heated channel with a Plexiglas tube of a very similar geometry, 1 m long and 25.6 mm I.D., under the same fluid-dynamic conditions. High speed movies of the flow (1000 fps) coupled with a digital image system allow to evaluate the slip ratio, and the void fraction, and to identify the flow pattern.

3. Heat transfer calculations

Available prediction correlations of the heat transfer coefficient, either in single-phase or in the nucleate boiling regime, are used for the reduction of single-component data (i.e., without air injection). The relationships used are reported in the following paragraph.

3.1. Single-phase flow

Most of the data lie in the turbulent mixed-convective flow region. This heat transfer regime occurs when the buoyancy forces (natural convection contribution) are of the same order of magnitude as the pressure gradient forces (forced convection contribution). The density difference between the near-wall region and the bulk liquid significantly modifies the velocity profile (Aung, 1987; Cotton and Jackson, 1990; Churchill, 1992), and in pipe vertical upflow, the buoyancy force tends to reduce the shear stress in the near-wall region, causing flow laminarization. A significant reduction in the heat transfer rate is experienced due to the laminarization effect. This behaviour rather complex may be described with the so-called 'two-layer model', as suggested by Aung (1987), depending on several thermal and geometrical parameters (see Cotton and Jackson, 1990). Conversely, as buoyancy force tends to increase the shear stress in the near-wall region, causing a heat transfer enhancement for downflow mixed-convection heated flow (see Churchill, 1992).

To calculate the heat transfer coefficient for upward-mixed convection heated flow conditions, the authors propose a new method following an approach recommended by Churchill (1992) for downflow, where the author postulates an overlapping of the contributions due to natural and forced convection. Churchill's method is modified for vertical heated upflow, to account for the decrease in the heat transfer due to the laminarization effect (see Celata et al., 1998). The heat transfer coefficient is given by:

$$h_{SC,sp} = \left(h_{for}^3 + h_{nat}^3\right)^{1/3} \Psi \tag{3}$$

$$\Psi = 1 - a\exp\left\{-0.8\left[\log(Bo/b)\right]^2\right\}; \quad a = 0.36 + 0.0065\frac{L}{D}, b = 869\left(\frac{L}{D}\right)^{-2.16}$$

$$h_{for} = 0.023\frac{k}{D}Re_b^{0.8}Pr_b^{0.4}\left(\frac{\mu_b}{\mu_w}\right)^{0.11} \tag{3a}$$

(Dittus–Boelter equation, see McAdams, 1983)

$$h_{nat} = \frac{0.15\dfrac{k}{D}(Gr_t Pr_w)^{1/3}}{\left[1 + (0.437/Pr_w)^{9/16}\right]^{16/27}} \tag{3b}$$

(Churchill, 1992)

$$Gr_t = \frac{g\beta(T_w - T_b)D^3}{\left(\mu_w/\rho_w\right)^2}; \qquad Bo = 8 \times 10^4 \frac{Gr_h}{\left(Re_f^{3.425} Pr_f^{0.8}\right)}; \quad Gr_h = \frac{g\beta q'' D^4}{\mu_f^2 k_f}$$

where, the buoyancy parameter, Bo, is given by Cotton and Jackson (1990). In Eqs. (3)–(3b) h is heat transfer coefficient, the subscript b refers to bulk, w to wall and f to film conditions (average between wall and bulk conditions), SC stands for single-component, sp for single-phase, for pertains to forced convective flow conditions and nat to natural convective flow conditions; $Pr = c_p\mu/k$ is the Prandtl number, μ is the dynamic viscosity, Gr_t and Gr_h are the Grashof numbers based on the temperature difference and the wall heat flux, k is the liquid thermal conductivity, g the gravitational acceleration, β the coefficient of volume expansion and T the temperature.

Once the heat transfer coefficient is calculated, the wall temperature is given by the heat balance:

$$T_{w,sp} = T_b + \frac{q''}{h_{SC,sp}} \tag{4}$$

3.2. Onset of nucleate boiling

The correlation proposed by Davis and Anderson (1966) is used to calculate the onset of nucleate boiling temperature, T_{ONB}:

$$T_{ONB} = T_{sat} + \left(\frac{8\sigma T_{sat} q''}{k_l \lambda \rho_g}\right)^{1/2} \tag{5}$$

where σ is the surface tension, T_{sat} the saturation temperature in Kelvin, q'' the heat flux delivered to the fluid, k_l the liquid thermal conductivity, λ the latent heat of vaporization, and ρ_g the steam density. The Bergles and Rohsenow (1963) correlation has also tested and provide a less accurate prediction of the current data.

3.3. Subcooled nucleate boiling

The nucleate boiling region in subcooled flow boiling may be further subdivided into two sub-regions, as shown in Fig. 3. The first is the so-called partially-developed subcooled boiling (B–E), where we have the convective contribution and that provided by the nucleation of the first bubbles growing at the wall. As the heat flux is increased, we enter the fully developed subcooled boiling region (E–F), where nucleation becomes predominant. The border between the two zones is uncertain. According to the Bergles and Rohsenow (1963) and the Steiner and Taborek (1992) models, they may be seen as a unique zone where the weight of the two heat transfer contributions (convection and nucleation) varies as a function of the heat flux, as sketched in Fig. 3(b).

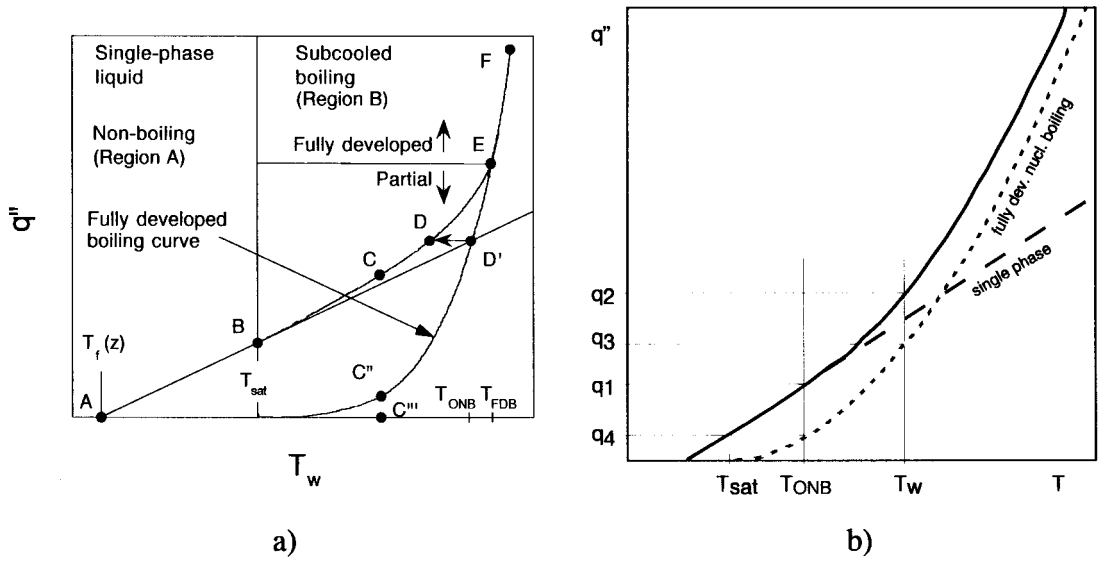

Fig. 3. (a) Subcooled boiling curve (Aung, 1987); (b) Bergles–Rohsenow method, Eq. (7).

3.3.1. Fully developed nucleate boiling

The heat transfer coefficient in the fully developed nucleate boiling region may be calculated using the Thom et al. (1965) correlation:

$$T_w = T_{sat} + 22.65\left(q''/10^6\right)^{0.5}\exp(-p/87) \tag{6}$$

where p is the system pressure, given in bar, while the heat flux, q'', is given in W/m^2, and T in °C.

The Shah's correlation (Shah, 1977) was also tested, providing a less accurate prediction of the current data.

3.3.2. Partially developed nucleate boiling

The method proposed by Bergles and Rohsenow (1963) is adopted in the current study. For known wall temperature T_w, the heat flux delivered to the fluid in the test section (q_2) is given by:

$$q_2^2 = q_1^2 + (q_3 - q_4)^2 \tag{7}$$

where, as shown in Fig. 3(b), q_1 is the single-phase heat flux at T_{ONB} (Eq. (3a)), q_3 is the heat flux at T_w in fully developed nucleate boiling (Eq. (6)), and q_4 is the heat flux for T_{ONB} (Eq. (6)). The method proposed by Bergles and Rohsenow (1963) consists in summing the contributions of the convective heat transfer (Eq. (3a)) and of the nucleate boiling heat transfer (Eq. (6)) so that for $T = T_{ONB}$ the calculated value is that due to convection only.

In the present case q_2 is experimentally known, q_4 and q_1 are calculated as detailed above, and q_3 can be found from Eq. (7).

3.4. Flow pattern and flow parameters

The flow pattern is evaluated using the maps suggested by Mishima and Ishii (1984), Taitel et al. (1980), and Costigan and Whalley (1997). The injection of air in the liquid phase causes a two-phase two-component flow, the characteristics of which may be evaluated from the flow pattern maps. As most of the data points are in the slug flow regime, the void fraction is calculated by the drift–flux model (see Wallis, 1969). According to the results of the flow pattern visualization, the homogeneous model can never be applied.

4. Experimental results

4.1. Heat transfer tests without air injection

Fig. 4 depicts some tests carried out without air injection. The experimental and calculated wall temperatures are plotted versus the heat flux, according to the methods described in the previous paragraph. For single-phase flow the agreement between experimental and calculated (Eqs. (3) and (4)) wall temperatures is good. Good agreement is also observed for $T_{w,exp} \gg T_{ONB}$, i.e., for subcooled boiling, either partially or fully developed.

A larger discrepancy is observed, instead, whenever the wall temperature is close to the saturation temperature. In this case the calculated wall temperature overestimates the experimental temperature. This discrepancy is explained by the presence of the air dissolved into the water. The test procedure (alternate running of tests with and without air injection) causes air to be always dissolved in water at the saturation conditions defined by the thermodynamic state. The influence of dissolved gas on the heat transfer has been already studied in the past (Collier and Thome, 1994; Asmolov et al., 1989). The dissolved gas causes the wall temperature to be lower than that expected from degassed water. Dissolved gas has the maximum influence in the zone preceding the ONB (Onset of Nucleate Boiling) condition. The influence of the dissolved air may be due to: (a) the temperature increase, especially close to the heated wall, which facilitates water degassing, band the very small air bubbles enhance local turbulence and, consequently, the heat transfer; (b) the dissolved air makes the onset of boiling in the wall cavities easier; as a consequence, the value of the T_{ONB} decreases and the nucleate boiling regime may be anticipated. The influence of dissolved air on the onset of nucleate boiling is reported in the literature, as already mentioned, but no method for its prediction or calculation is available so far.

The ratio between the experimental and the calculated heat transfer coefficient is reported in Fig. 5 versus the heat flux, for the tests without air injection. Taking into account the measurement error for the various experimental parameters used in the calculation of the heat transfer coefficient for tests without air injection, the latter is affected by an experimental uncertainty less than 19%. Data points referring to a calculated temperature higher than the saturation values are distinguished from the ones referring to a calculated temperature lower

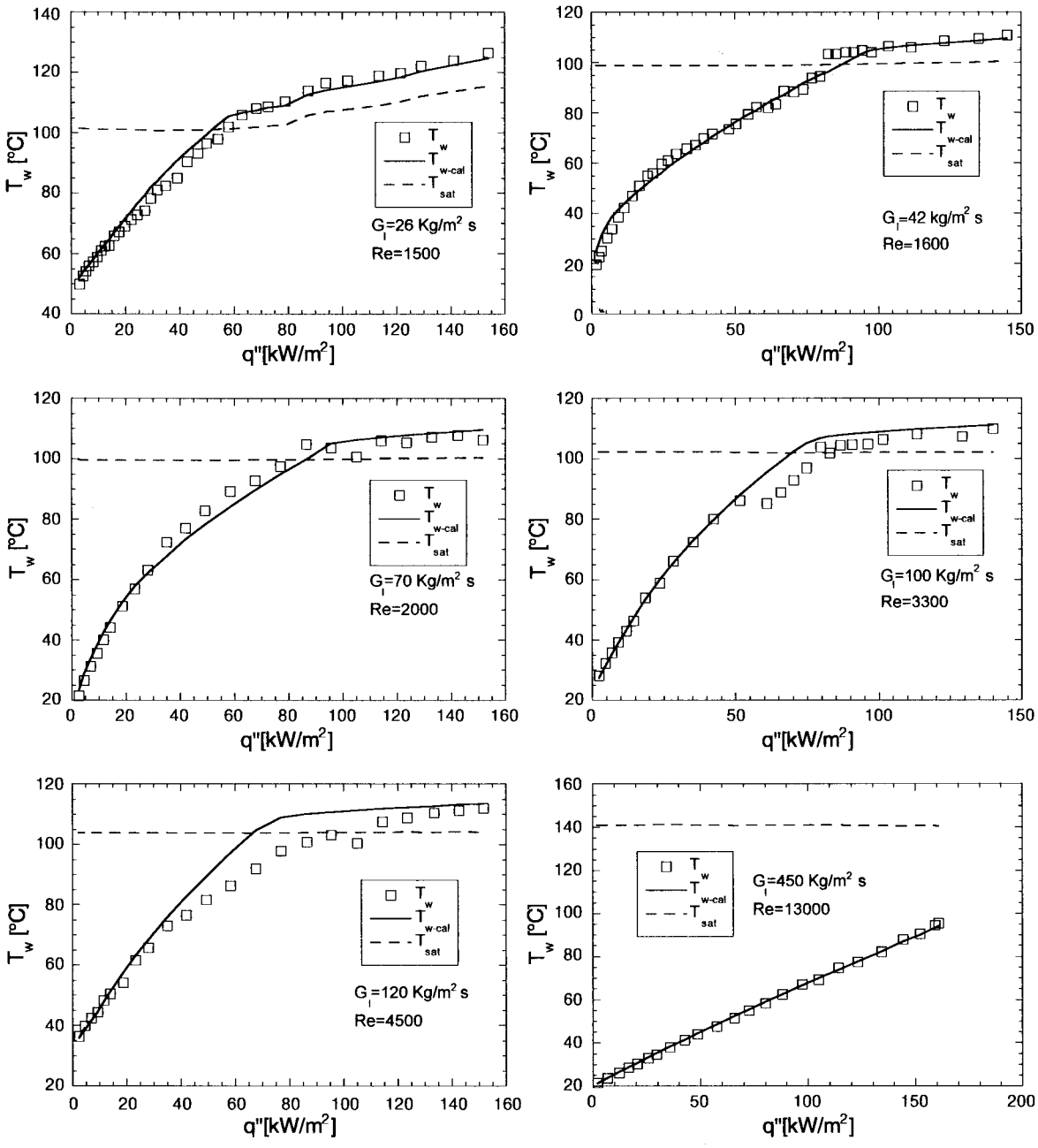

Fig. 4. Comparison between experimental and calculated wall temperatures as function of the heat flux, for tests without air injection.

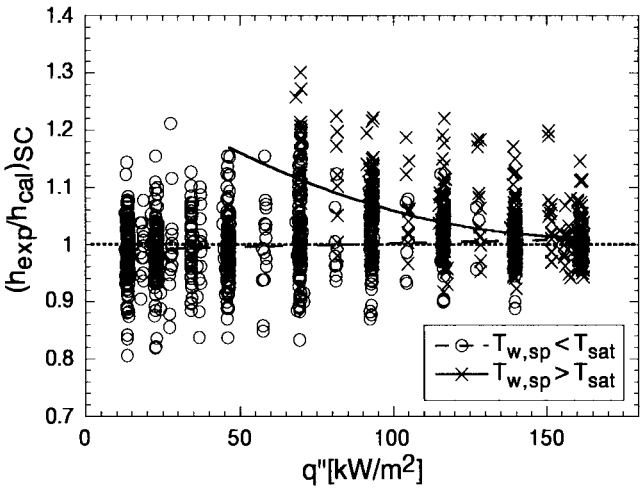

Fig. 5. Experimental to calculated heat transfer coefficient ratio vs. heat flux (runs without air injection).

than the saturation. For the two classes of data, a best-fit line is traced. The average error is equal to zero for $T_w < T_{sat}$ (dotted line), while for $T_w > T_{sat}$ it increases as the heat flux decreases (continuous line), which can be explained by the above considerations on dissolved gas. Soon after saturation conditions are reached near the wall region, dissolved gas bubbles start leaving the liquid, while steam bubbles start growing at the wall. Gas and steam bubbles tend to increase the turbulence level at the near-wall in the downstream region, where, therefore, the heat transfer coefficient increases and the wall temperature can settle down in the saturation value. Bubble presence is also directly detected, visualizing the flow few centimeters downstream from the exit of the test section. As the heat flux is further increased after ONB, nucleate boiling tends to control the heat transfer. The behaviour can be again well predicted using the above reported correlations.

4.2. Heat transfer tests with air injection

The influence of air injection in the liquid flow is shown in Figs. 6–9. Taking into account the measurement error for the various experimental parameters used in the calculation of the heat transfer coefficient for tests with air injection, the latter is affected by an experimental uncertainty less than 17%. Fig. 6 shows similar tests to evaluate both the influence of air injection, and of the air injection mode. Ratio between the experimental and the calculated value of the heat transfer coefficient is plotted versus the heat flux two-component mixture (air and water) in the upper part of each graph (indicated with TC), and for the single-component flow (water only) in the lower part (indicated with SC). The calculated heat transfer coefficient is obtained using the correlations available for single-component flow, i.e., Eq. 3. In view of the good agreement between single-component data points and predictions obtained using Eq. (3), points for two-component data (i.e., with air injection) represent with a good approximation for the ratio between the experimental two-component heat transfer coefficient and the corresponding single-component experimental value. Tests are carried out increasing

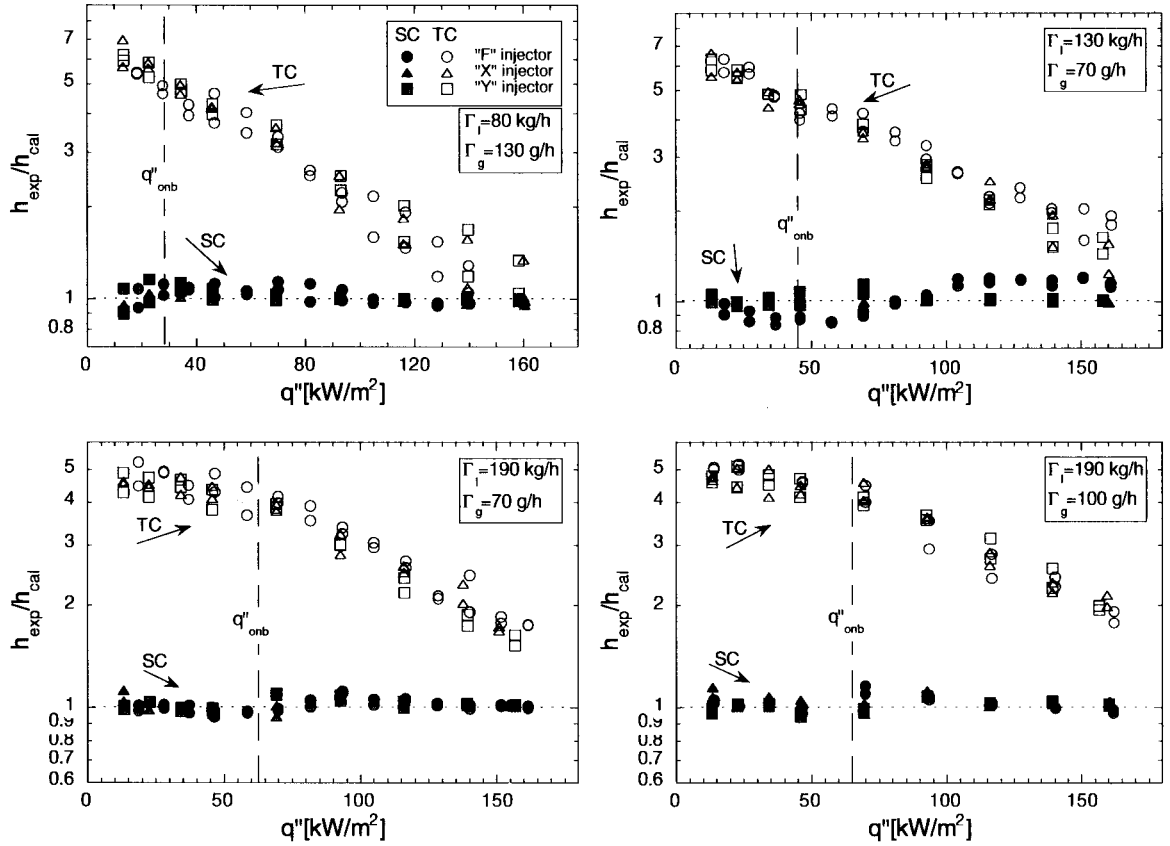

Fig. 6. Experimental-to-calculated heat transfer coefficient ratio vs. heat flux. Effect of the air injection mode, and effect of the air injection rate on the heat transfer rate. Typical tests at $p = 1.5$ bar (TC = two-component flow; SC = single-component flow).

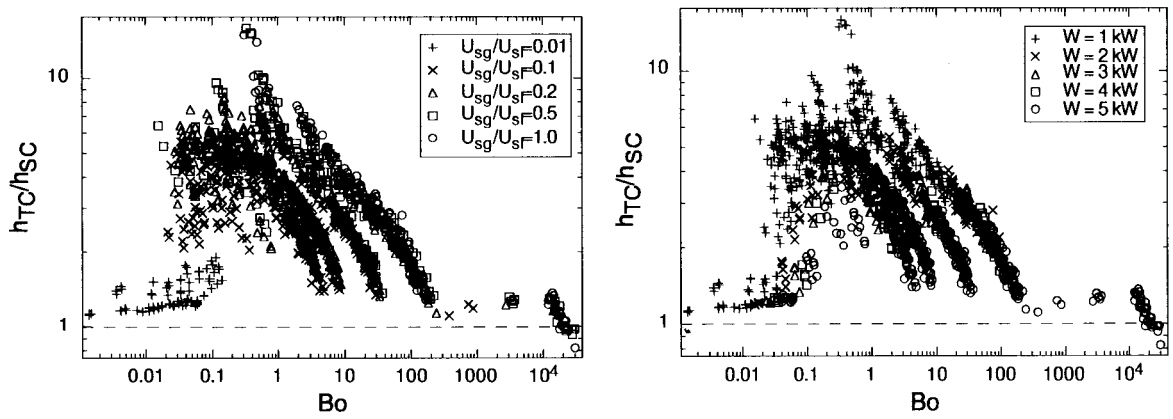

Fig. 7. Heat transfer coefficient with air injection (TC) and without air injection (SC) vs. the buoyancy parameter, for different values of the gas-to-liquid superficial velocity ratio (left-hand side graph) and the total thermal power delivered to the fluid (right-hand side graph).

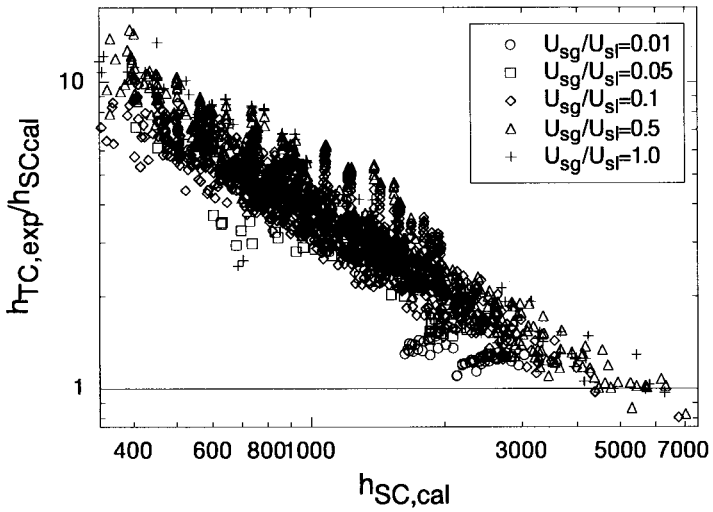

Fig. 8. Effect of air injection on the heat transfer coefficient.

the heat flux for fixed values of air and water flow rate. The air injection mode does not affect the heat transfer coefficient, as data obtained with the three air injection modes lie on a single curve. Air injection may enhance the heat transfer rate up to almost one order of magnitude, due to the turbulence increase in the fluid flow. As the heat flux is increased, the effect of the air injection tends to decrease until it vanishes for high heat fluxes. In fact, as the heat flux increases, the turbulence of the flow increases as well, due to the near-wall bubble generation. Once the ONB heat flux, q''_{ONB}, has been reached, the air injection effects tends to decrease more rapidly as the heat flux increases, vanishing when saturated boiling conditions are approached. The data points plotted in Fig. 6 are a subset of those collected during the whole experimental campaign. These tests are carried out with the main purpose to ascertain any possible influence of the air injection mode on the results.

In Fig. 7 the ratio between the heat transfer coefficient with air (TC) and that without air (SC) are plotted versus the buoyancy parameter, *Bo* (Eq. (3)). The parameters of the two graphs are: (1) the ratio between the gas and the liquid superficial velocity, which is a measure of the injected air mass flow rate, and (2) the total thermal power delivered to the fluid. The buoyancy parameter, which represents the ratio between the buoyancy and the pressure gradient forces, allows one to estimate the convection type in the fluid flow. Roughly, for $Bo<0.02$–0.05 forced convection flow is established. Conversly natural convection may be experienced for $Bo > 50$–100; in between mixed-convection flow takes place. From Fig. 7 it is quite clear how the air injection effect is significant where the flow condition is of the mixed-convection type, as the heat transfer coefficient is up to 10 times higher than without air injection. As already discussed above, and extensively described by Celata et al. (1998), mixed convection in upward heated flow is characterized by a laminarization effect (the effect is maximum when *Bo* is around 1, and is due to the buoyancy effect on the velocity and shear stress profiles) which greatly reduces the heat transfer rate. The main effect of air injection is that of destroying the velocity profile in the fluid flow, suppressing the laminarization effect

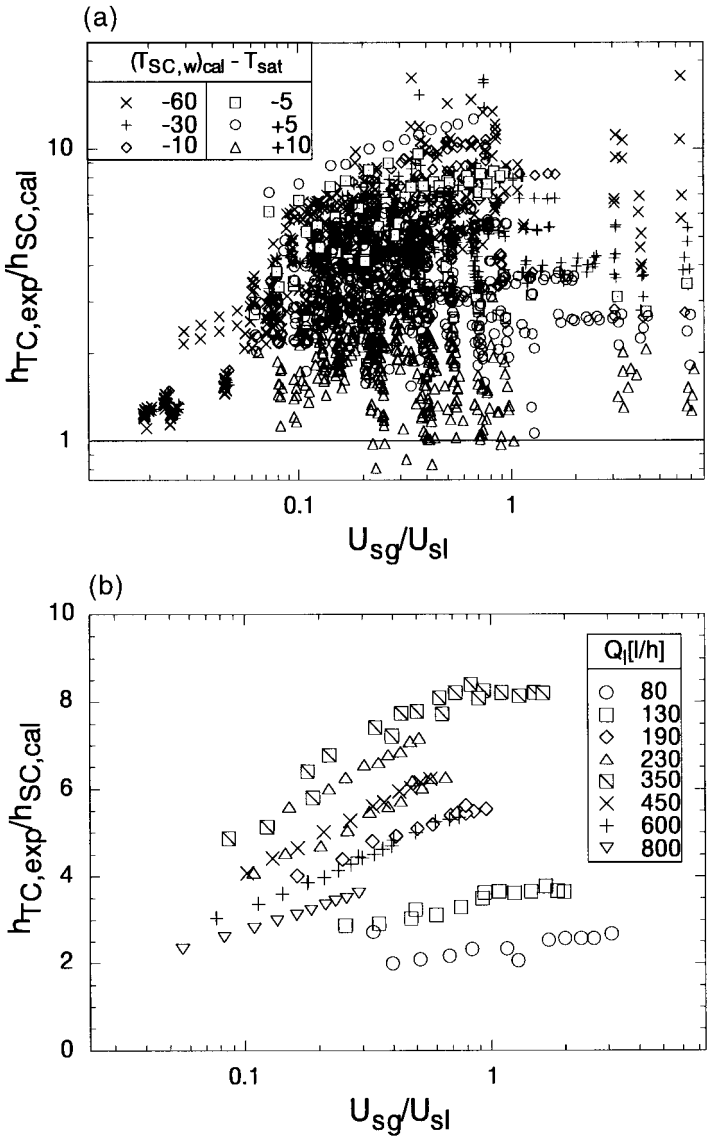

Fig. 9. Effect of air injection vs. the gas-to-liquid superficial velocity ratio: (a) the grouping parameter being the difference between the calculated wall temperature and the saturation temperature, and (b) the grouping parameter being the volumetric flow rate, for $q'' = 64$ kW/m^2.

and enhancing heat transfer. Flow visualization of the air–liquid flow shows this feature and provides the information on the flow pattern, which is of the slug flow type for most of the data points. For pure natural ($Bo > 100$) and forced convection ($Bo<0.02$), the effect of air injection on the heat transfer coefficient, although detectable, is reduced to only 20–40%, vanishing for $Bo > 10^4$ (actually reducing the heat transfer rate). When the flow is fully turbulent, the effect of air injection on the turbulence itself will be definitely low as expected.

For a given value of *Bo*, and for convection flow, the effect of the air injection would seem to be an increasing function of the air mass flow rate (proportional to U_{sg}/U_{sl}, where these are the gas and liquid superficial velocities, respectively) and inversely proportional to the heat flux delivered to the fluid, as already observed in Fig. 6.

Fig. 8 shows all the performed test; the ratio between the two- and single-component flow heat transfer coefficients is plotted versus the single-component flow heat transfer coefficient, grouped by the U_{sg}/U_{sl} ratio, h_{SC} being a reasonable measure of liquid turbulence due to the combination of the Reynolds number and onset of nucleate boiling effects on the turbulence itself. The maximum increase in the heat transfer rate is about 10 times, attainable for a small value of the heat transfer coefficient for single-component flow, e.g., mixed convection in upward heated flow.

The ratio between the experimental values of the heat transfer coefficient with (TC) and without (SC) air injection is plotted in Fig. 9 versus the U_{sg}/U_{sl} ratio. Data are grouped according to the difference between the calculated wall temperature and the saturation temperature, Fig. 9(a), and according to the liquid volumetric flow rate, Fig. 9(b). Fig. 9(a) shows how the heat transfer coefficient enhancement due to air injection is maximum when the wall temperature is lower than the saturation value. As the wall temperature approaches the saturation temperature, the heat transfer enhancement decreases, until it disappears when subcooled boiling becomes the governing phenomenon in heat transfer, and the initial turbulence level is high enough to be insensitive of air injection. Fig. 9(a) and (b) also show that the effect of the air flow rate on heat transfer enhancement is larger for low values of the air flow rate itself, tending to vanish as the U_{sg}/U_{sl} ratio increases (and then the air mass flow rate increases too) tending to unity. For a fixed value of the U_{sg}/U_{sl} ratio and of the heat flux for the data plotted (64 kW/m^2 in Fig. 11), the heat transfer coefficient enhancement due to air injection increases with the liquid mass flow rate, and it reaches a maximum (for 350 l/h) and then decreases as the liquid mass flow rate is further increased. As shown in Fig. 7, the maximum influence of air injection on the heat transfer takes place for mixed-convection flow conditions.

The heat transfer coefficient with air injection can be simply calculated using the following relationship:

$$h_{TC} = 2176\, h_{SC}^{0.11}\left(1 + 0.19 \log\frac{U_{sg}}{U_{sl}}\right) \tag{8}$$

This simple equation takes into account the turbulence level before air injection, including the convection flow type, through h_{SC} (ranging from 450 to 6500 W/m^2 K), and with the direct effect of air injection through the U_{sg}/U_{sl} ratio.

The comparison between predictions and experimental values is reported in Fig. 10, the calculated versus experimental heat transfer coefficients (left graph), and the ratio between the calculated and the experimental heat transfer coefficients versus void fraction (right graph). Most data lie within $\pm 20\%$, with a standard deviation of 14.0%.

As an evaluation of the proposed enhancement technique, with respect to other existing techniques, the hypothetical efficiency of twisted tape inserts is calculated under the same conditions, using the Lopina and Bergles, 1969:

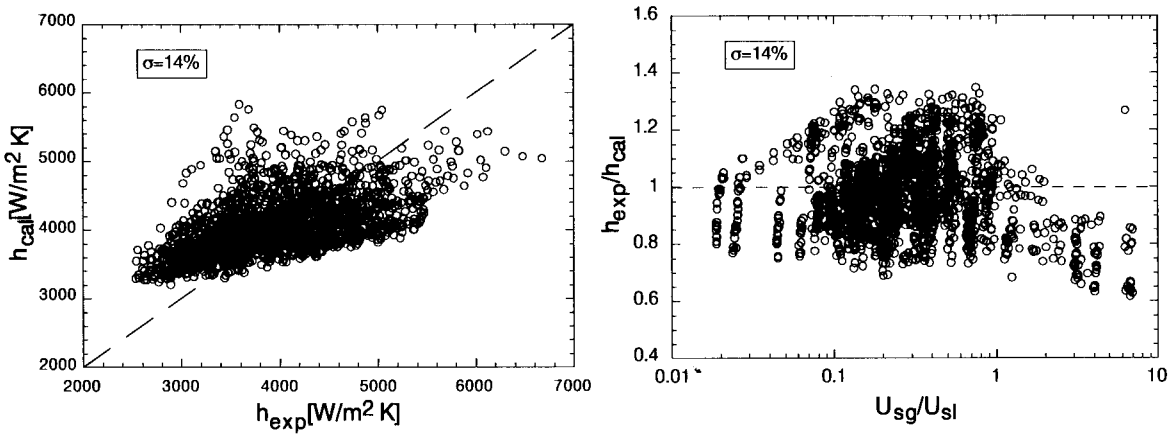

Fig. 10. Prediction of the heat transfer coefficient using correlation (8).

$$h_{tt} = 0.023\frac{k}{D_h}\left[1+\left(\frac{\pi}{2y}\right)^2\right]^{0.4} Re_h^{0.4} Pr_h^{0.4} + 0.193\left(\frac{Re_h}{y}\right)^2 \frac{D_h}{D}(T_w - T_b)\beta\, Pr^{0.5} \tag{9}$$

Where D_h is the hydraulic diameter, and y is the twisted-tape ratio.

Fig. 11(a) shows the comparison between h_{tt} and the corresponding calculated heat transfer coefficient obtained using the Dittus–Boelter correlation versus Reynolds number. Fig. 11(b) shows the comparison between h_{tt} and the corresponding experimental heat transfer coefficient obtained with air injection, h_{TC}, versus Reynolds number. The heat transfer enhancement provided by air injection is more effective than swirl flow for low-Reynolds number, when the flow is under low turbulence conditions. Twisted-tape inserts are more effective at higher Reynolds numbers, because, as passive devices, they increase turbulence proportionally to the flow velocity, thanks to the swirl flow.

5. Visual observations

From adiabatic tests carried out with the Plexiglas test section, information about the flow pattern after air injection is obtained. Typical pictures are reported in Fig. 12, where for a liquid volumetric flow rate of 60 l/h, different air flow rates are observed. They range from 50 to 708 l/h going from the left to right, corresponding to 60.6 and 856.2 g/h, respectively. The pictures are taken at a distance of 35 cm from the test section inlet, while the portion of the tube in the pictures is about 40 cm. Slug flow is experienced very soon (air flow rate of 116 l/h, or 140.4 g/h, equivalent to a value of $U_{sg} = 6.28$ cm/s), while for the whole range of air flow rates the velocity profile in the pipe can possibly be destroyed by the passage of the bubbles. This continuous 'renewal' of the velocity profile due to bubble passage is the key to understanding the significant enhancement of the heat transfer in the mixed-convection regime, as experienced in the diabatic tests. The most important consequence of the bubble passage is

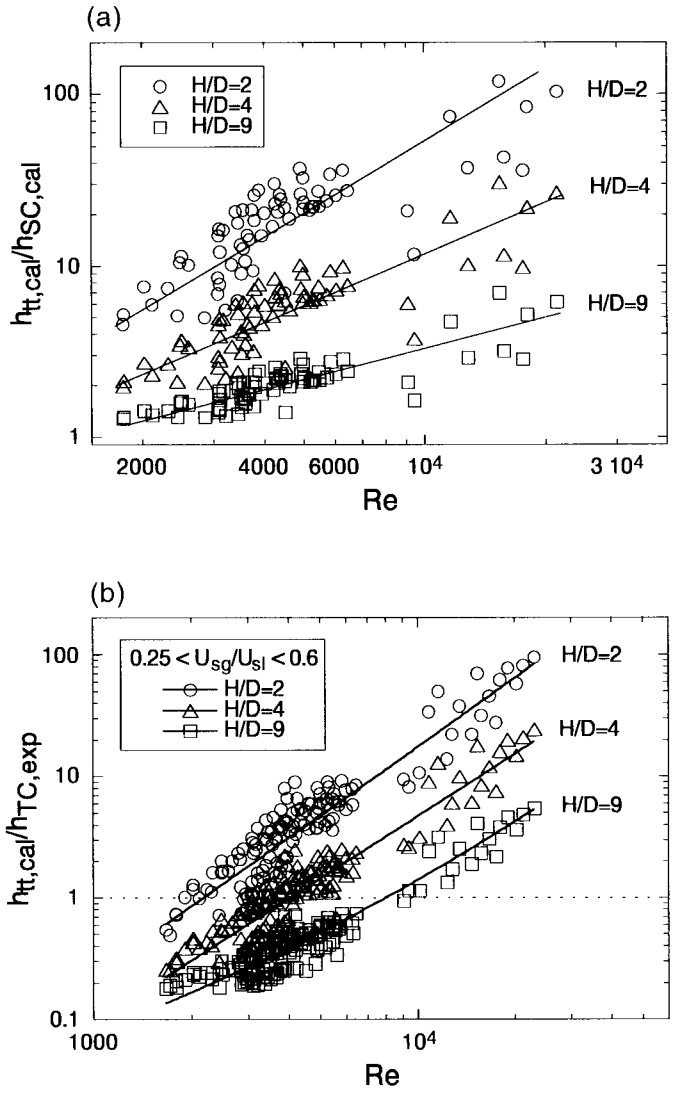

Fig. 11. (a) Enhancement of heat transfer using twisted-tape inserts; (b) comparison between twisted-tape inserts and air injection performance.

the suppression of the laminarization effect caused by the buoyancy and the subsequent restoration of a turbulence level able to provide a 'high heat transfer rate'.

Fig. 13 shows the prediction of the flow pattern for the visualized tests using the maps suggested by Mishima and Ishii (1984), Taitel et al. (1980), and Costigan and Whalley (1997). The Mishima and Ishii (1984) map (top graph) does not give a good prediction of the observed flow pattern, identifying all the spherical cup bubble flow data and part of the slug flow data as bubbly flow. On the other hand, Taitel et al. (1980) claim that for tubes smaller than 5.0 cm in diameter, no bubbly flow can exist for U_{sl} less than 1 m/s (for the present data). Predictions provided by the Taitel et al. (1980) map for $D = 2.5$ cm (middle graph) are more consistent

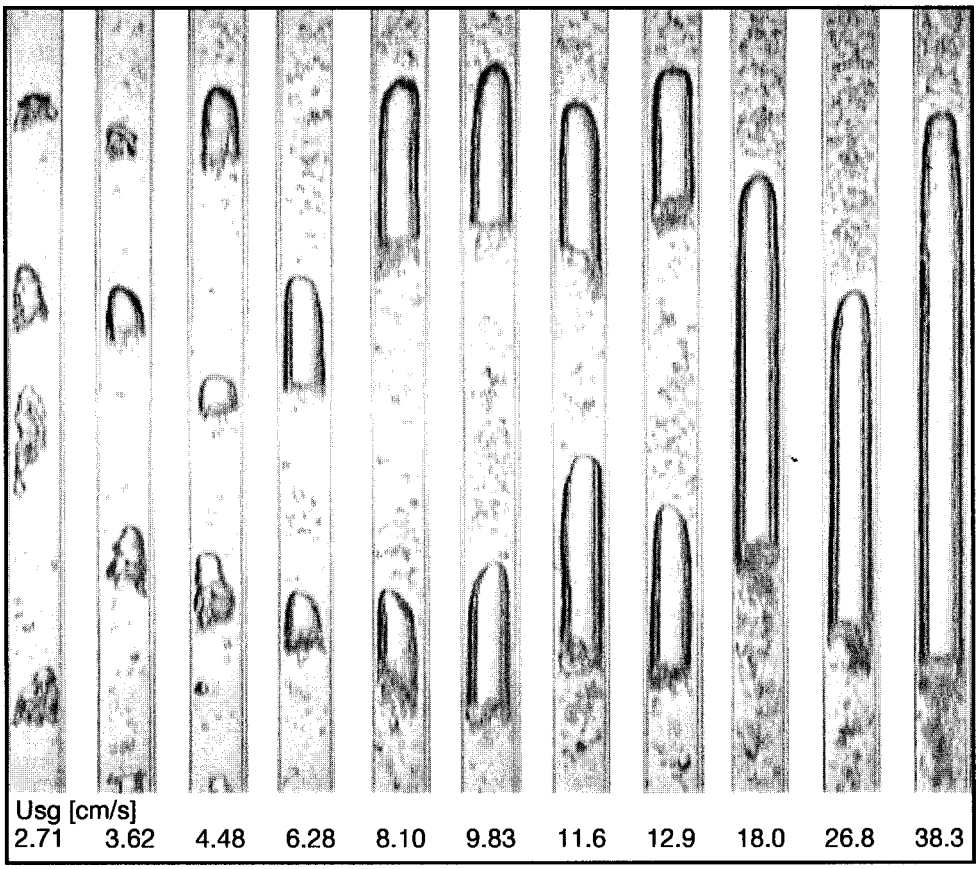

Fig. 12. Typical pictures of the flow pattern evolution, for a liquid volumetric flow rate of 60 l/h. The air volumetric flow rate ranges from 50 to 708 l/h (60.6 to 865.2 g/h).

with the present data, though the map generically indicates slug flow for all the data. Finally, the Costigan and Whalley (1997) map (bottom graph) provides a good prediction of the present data, also distinguishing between spherical cup bubble and slug flow.

6. Conclusions

The possibility of enhancing the heat transfer coefficient in a heated-duct water flow using an injection of air at the inlet of the heated channel is investigated. Such a possibility is especially welcome for mixed-convection in upward heated flow. Under these conditions, characterized by a very low heat transfer coefficient, air injection is proved to enhance the heat transfer coefficient up to a factor of 10, simply as a consequence of the suppression of the laminarization effect, responsible of the low heat transfer rate in upward mixed-convection flow. The turbulence increase due to air injection is observed also under forced-convection flow, where an increase of the heat transfer coefficient up to 20–40% is found.

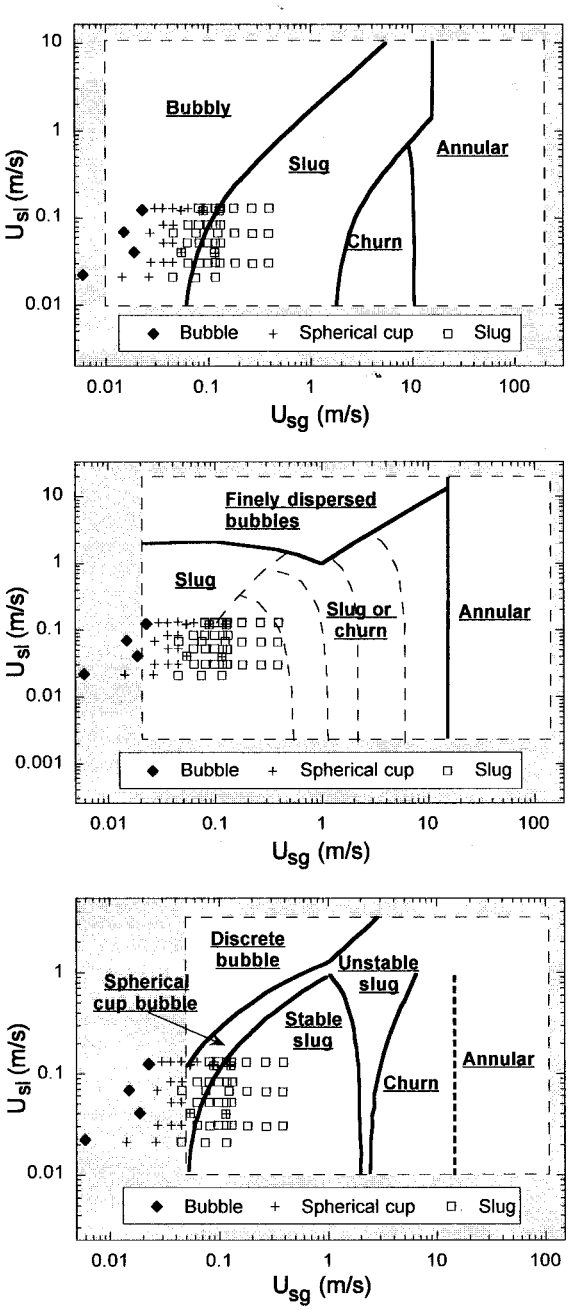

Fig. 13. Estimation of the observed flow pattern using the maps proposed by Mishima and Ishii (1984), Taitel et al. (1980), and Costigan and Whalley (1997) (from top to bottom).

Visual studies carried out using a Plexiglas tube show that, under the tested fluid-dynamic conditions, the flow pattern is sluggish for most of the tests. The spherical-cup bubble flow is experienced for the remaining tests. The flow patterns, well predicted by the Taitel et al. (1980) and Costigan and Whalley (1997) maps, cause the continuous renewal of the velocity profile in the cross section, suppressing the laminarization effect typically occurring in upward mixed-convection flow. The consequent increase of the turbulence level is the reason of the enhancement of the heat transfer rate.

For small air mass flow rates, the heat transfer enhancement depends on the air flow rate, but it tends to stabilize as the air flow rate is further increased.

References

Asmolov, V.G., Yelkin, I.V., Kobzar, L.L., 1989. The effect of gas dissolved in the water on heat transfer coefficients in nuclear reactors. Heat Transfer-Soviet Research 21, 810–819.

Aung, W., 1987. Mixed convection in internal flow. In: Kakaç, S., Shah, R.K., Aung, W. (Eds.), Handbook of Single-Phase Convective Heat Transfer. Wiley, New York, pp. 15.1–15.47.

Bergles, A.E., Rohsenow, W.M., 1963. The determination of forced convection surface boiling heat transfer. In: 6th National Heat Transfer Conference of the ASME-AIChE, Paper 63-HT-22, Boston.

Celata, G.P., Chiaradia, A., Cumo, M., D'Annibale, F., 1998. Heat transfer in upward mixed convective flow of water in vertical pipe. In: Proc. 11th International Heat Transfer Conference, Kyongju, Korea, 23–28 August.

Churchill, S.W., 1992. Combined free and forced convection in channels. In: Hewitt, G.F. (Ed.), Handbook of Heat Exchanger Design. Begell-House, paragraph 2.5.10.

Collier, J.G., Thome, J.R., 1994. Convective Boiling and Condensation. Oxford Science Publications, Clarendon Press, Oxford pp. 207–208.

Costigan, G., Whalley, P.B., 1997. Slug flow regime identification from dynamic void fraction measurements in vertical air–water flows. Int. J. Multiphase Flow 23, 263–282.

Cotton, M.A., Jackson, J.D., 1990. Vertical tube air flows in the turbulent mixed convection regime calculated using a low Reynolds number k-ε model. Int. J. Heat Mass Transfer 33, 275–286.

Davis, E.J., Anderson, G.H., 1966. The incipience of nucleate boiling in forced convection flow. AIChE Journal 12, 774–780.

Du Plessis, J.P., Kroger, D.G., 1987. Heat transfer correlation for thermally developing laminar flow in a smooth tube with a twisted-tape insert. Int. J. Heat Mass Transfer 30, 509–515.

Lopina, R.F., Bergles, A.E., 1969. Heat transfer and pressure drop in tape-generated swirl flow of single-phase water. J. Heat Transfer 91, 434–442.

McAdams, W.H., 1983, Heat Transmission. McGraw Hill, New York p. 219.

Mishima, K., Ishii, M., 1984. Flow regime transition criteria for upward two-phase flow in vertical tubes. Int. J. Heat Mass Transfer 27, 723–737.

Oliver, D.R., Aldington, R.W.J., May 1992. Enhancement of laminar flow heat transfer using wire matrix turbulators. In: 8th Int. Heat Transfer Conf., San Francisco, vol. 6, 2897–2902.

Shah, M.P.E., 1977. A general correlation for heat transfer during subcooled boiling in pipes and annuli. ASHRAE Trans. 83 (1), 202–217.

Steiner, D., Taborek, J., 1992. Flow boiling heat transfer in vertical tubes correlated by an asymptotic model. Heat Transfer Engineering 32, 43–69.

Taitel, Y., Barnea, D., Dukler, A.E., 1980. Modelling flow pattern transitions for steady upward gas–liquid flow in vertical tubes. AIChE Journal 26, 345–354.

Thom, J.R.S., Walker, W.M., Fallon, T.A., Reising, G.F.S., 1965. Boiling in subcooled water during flow up heated tubes or annuli. Paper presented at the Symposium on Boiling Heat Transfer in Steam Generating Units and Heat Exchangers, Manchester, 15–16 September, IMechE, London.

Uttarwar, S.B., Raya Rao, M., 1985. Augmentation of laminar flow heat transfer in tubes by means of wire coil inserts. ASME Trans. 107, 930–935.
Wallis, G.B., 1969. One Dimensional Two-Phase Flow. McGraw-Hill, New York pp. 89–105.